

# Physical Twins: bridging the gap of minimal data and real-world human experiments

**Abstract**—Human-robot physical interaction (pHRI) is a rapidly evolving research field with significant implications for physical therapy, search and rescue, and telemedicine. However, a major challenge lies in accurately understanding human constraints and safety in human-robot physical experiments without an IRB and physical human experiments. Concerns regarding human studies include safety concerns, repeatability, scalability of the number, and diversity of participants. This paper examines whether a physical approximation can serve as a stand-in for human subjects to enhance robot autonomy for physical assistance. This paper introduces the SHULDRD (Shoulder Haptic Universal Limb Dynamic Repositioning Device), an economical and anatomically similar device designed for real-time testing and deploying pHRI planning tasks on robots in the real world. SHULDRD replicates human shoulder motion, providing crucial force feedback and safety data. The device’s open-source CAD and software facilitate easy construction and use, ensuring broad accessibility for researchers. By providing a flexible platform able to emulate infinite human subjects, ensure repeatable trials, and provide quantitative metrics to assess the effectiveness of the robotic intervention, SHULDRD aims to improve the safety and efficacy of human-robot physical interactions.

## I. INTRODUCTION

Numerous tasks, including home assistive care, telemedicine, casualty extraction, and physical therapy, could benefit greatly from the addition of physical robotic assistance, specifically assistance with tasks involving moving the human body. Work has shown promise for assisting with dressing [1] by holding and moving clothes and weight shifting [2] by tugging on bed sheets as a proxy to grasping and lifting the person. While these tasks push robotic assistance forward, they are missing human contact due to the challenge of conducting human trials and safety concerns.

In medical diagnostics, there have been research and commercial implementations of impedance and admittance controllers that allow the robot to follow the contour of a patient with a model for the safety of human soft tissue. In research, there has been work to teleoperate and automate heart listening [3] and automate arthritis diagnosis with ultrasound [4]. Similarly, these controllers are used for human-robot collaboration physical therapy tasks [5]. However, there is still a lack of a method for achieving dexterous manipulation in interactions with people. Being able to grasp, tug, and maneuver the human body would dramatically increase the type of assistance robots could provide, as shown in [6] for search and rescue tasks.

An area in which this type of contact is currently prevalent is wearable assistance technology. Many are cleverly

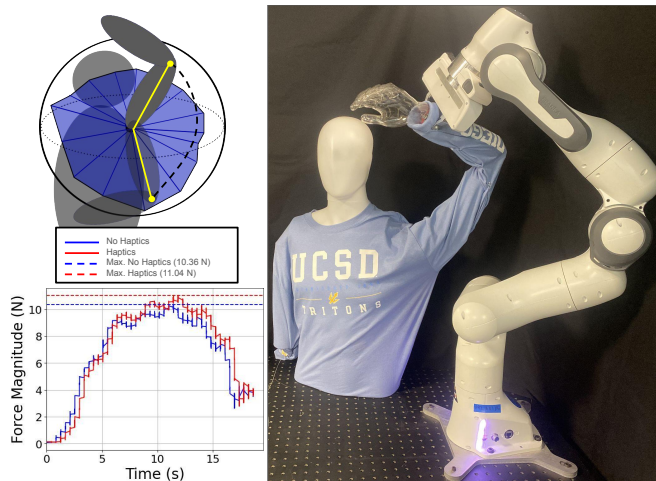


Fig. 1: SHULDRD used in a human-robot physical interaction experiment where SHULDRD simulates a human shoulder. The image on the upper left shows the shoulder position relative to its complex spherical joint limits. The graph on the lower left shows the activation of the actuators, rendering the elastic forces that mimic those produced by human tendons when the arm goes beyond its reachable space.

designed to align with and move with the wearer’s natural anatomy, utilizing exoskeleton technology and advanced high-fidelity human modeling to optimize design. However, human intervention does not provide adequate protection. Studies show that bone fractures and skin and soft tissue damage from lower limb exoskeletons are a risk of device use [7]. The sim-to-real gap of high-fidelity human models and the high variance across real humans can lead to these injuries. This lesson from wearable technology begets the necessity for real-world online learning and greater consideration for user variation in addition to close human models.

As the previous example shows, robots must first properly understand safety to achieve their full potential in these tasks: end ranges of motion in joints, soft tissue damage [8], and dislocations in the complex joint spaces of the human body. An ideal physical model would render enough information and variable cases to ensure robust and safe robotic trajectories without risk to a human subject.

The next roadblock is the means to evaluate this safety. There are designs on the market for robotic shoulders that mimic or are inspired by human anatomy. Humanoids are one example, and some manipulators could be considered shoulder-like with their similar range of motion achieved through redundant degrees of freedom. For human replacement in pHRI, neither humanoids nor serial link robotic manipulators are ideal. They are designed for actuation, not rendering virtual environments, and are costly if damaged.

TABLE I: Requirements for Haptic Shoulder Platform

num	Requirement
1	singular joint center (no series linkage designs)
2	maximize reachable space of shoulder to ensure coverage of entire human shoulder range of motion
3	ability to give force feedback in 3D space of the shoulder joint
4	measures the position of the shoulder with greater accuracy than traditional vision systems
5	ensure forces rendered are safe for operators and robotic arms that may be used in experiments

A simple and economical haptic shoulder is proposed to test human-robot physical interaction planning tasks to bridge this gap. The device is designed to replicate the anatomical range of motion of the human shoulder joint so that human participants do not need to be used as test and development subjects. An additional key benefit will be providing force feedback, customizable individual user parameters, and data unavailable from a human subject, which can be used to enhance learning algorithms and safety. The CAD is open source and simplified for construction by researchers with non-mechanical backgrounds. The materials used are chosen for their flexibility and low cost. The software is open source and includes models for the shoulder complex reach cone joint limits.

To make a useful device for pHRI, there are essential characteristics the device must include to replicate the most important aspects of human anatomy critical for the safety of the human, real-world path planning experiments, and the safety of the robotic system being used. These requirements are listed in Table I.

The final system, referred to as SHULDRD (Shoulder Haptic Universal Limb Dynamic Repositioning Device), is presented with a clear analysis of how it compares to the desired capabilities.

## II. METHODS

To make a useful device for pHRI, there are essential characteristics the device must include to replicate the most important aspects of human anatomy critical for the safety of the human, real-world path planning experiments, and the safety of the robotic system being used. These requirements are listed in Table I.

The final system, referred to as SHULDRD (Shoulder Haptic Universal Limb Dynamic Repositioning Device), is presented with a clear analysis of how it compares to the desired capabilities.

Given the limited data for individuals, the joint limits will be made by collecting participants' 3 ranges of motion: flexion/extension, adduction/abduction, and internal/external humeral rotation. The four ranges are then used to generate a discrete dataset of possible configurations for human shoulders. While more thorough methods can equally produce ranges of motion, for example, sign distance fields, they require far more data and are often made with aggregate data from multiple people. In this system, the goal is to render the unique ranges of motion across individuals.

### A. Modeling Safety: Reach Cone Constraints for Biomechanically Accurate Joint Limits

Spherical joints pose a challenge in defining joint limits as they can not be defined with box limits. Box limits are

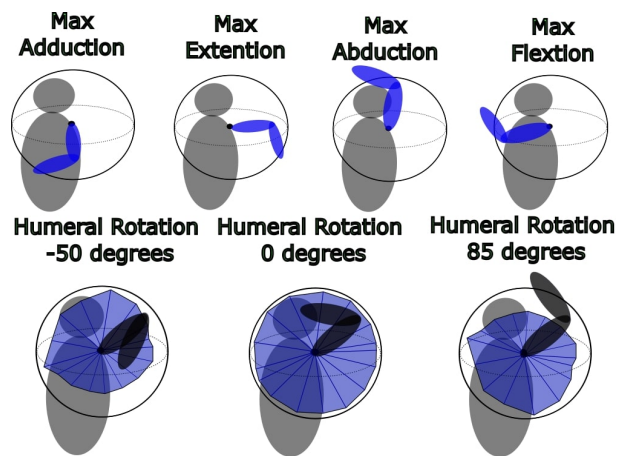


Fig. 2: A reach cone starts as 4 angles defining the maximum ROM in each direction. These 4 angles shown in the top 4 images define points on the unit sphere:  $[p_1, p_2, p_3, p_4] \in \mathcal{P}$ , where  $\mathcal{P}$  is the set of points on the unit sphere defining the joint limits. The second row of images shows different reach cones at different humeral orientations

defined as linearly independent  $[min, max]$  pairs. These are used for serial linkage and manipulators, but cannot describe complex joint limits in which the joint limits are interdependent on the current configuration. The shoulder joint limits would be written as such:

$$\begin{aligned}
 \Gamma_{free} &= [\gamma_{min}, \gamma_{max}] = f_{\gamma}(\theta, \phi) \\
 \Theta_{free} &= [\theta_{min}, \theta_{max}] = f_{\theta}(\phi, \gamma) \\
 \Phi_{free} &= [\phi_{min}, \phi_{max}] = f_{\phi}(\theta, \gamma)
 \end{aligned} \tag{1}$$

where  $\Gamma_{free}$ ,  $\Theta_{free}$ ,  $\Phi_{free}$  are the joint ranges of motion and  $\gamma$ ,  $\theta$ ,  $\phi$  are the current configuration: humeral rotation, flexion angle, and abduction angle, respectively.

Due to the asymmetry of the humeral head, it is non-trivial to produce an analytical solution for the coupling between the ranges of motion. Instead, most implementations use large data models. In this paper, joint limits are calculated using the reach cone method to minimize memory usage. In applying this method, the coupling function for humeral rotation is assumed to be constant.

1) *Defining the Joint Limits as a Reach Cone:* The reach cone is a discretized set of vectors defining the acceptable orientation region. Data on human shoulder range of motion is typically collected via goniometer data, which only represents four angles, the maximum range of motion for flexion, extension, abduction, and adduction, shown in the top row of Fig. 2. The average maxima can be found in Table ?? [9]. To establish a cone shape, the data was interpolated to create a total of 64 unit vectors or points on the unit sphere, shown in the second row of Fig. 2 where each cone is shown with a different humeral orientation affecting the cone shape.

2) *Virtual Tendon Stretch Calculation:* As shown in equations 8 and 9, it is necessary to calculate the angular error or angular distance from the joint limits.

Calculating the inclusion of a specific state,  $\theta$ , within the reach cone efficiently involves a series of steps outlined in [10]. The first is to define a visible vector or point that is in  $\Theta_{free}$  and defines the other half of the sphere shown in Fig.

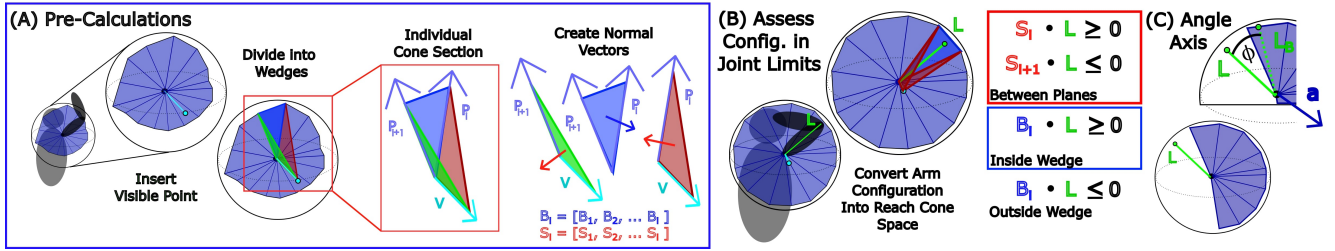


Fig. 3: In part (A), "Pre-Calculations" the figure shows the addition of the visible,  $V$ , in cyan, placed in the reach cone to designate the internal region. The visible point is then used to divide the internal space into wedges, one of which is depicted in its three surfaces, red, blue, and green. These surfaces are saved as surface normals  $B_i$  and  $S_i$ , depicted in blue and red. Section (B) shows the calculation to define whether a shoulder orientation belongs in the reach cone. Section (C) shows the final analysis needed for when an orientation is found outside the cone and needs to be pushed back towards the cone in the appropriate direction.

3 (A), which is the reachable space. Next, we calculate all the surface normals of the wedges that comprise the reach cone:

$$B_i = P_i \times P_{i+1} \quad (2)$$

$$S_i = V \times P_i \quad (3)$$

where  $P_i \in \mathcal{R}^3$  is the unit vector formed from the joint center to the point defined as part of the edge of the reach cone,  $B_i \in \mathcal{R}^3$  is the surface normal of the edge triangle with the positive direction pointing into the cone,  $S_i \in \mathcal{R}^3$  is the surface normal of the internal surfaces subdividing the cone and  $V \in \mathcal{R}^3$  is the visible point vector, the vector within the reach cone used to help subdivide the space.

Fig. 3 (A) next shows the surfaces that are formed from the  $P_i$ ,  $P_{i+1}$ , and  $V$  vectors. The  $P_i$  vectors are shown in purple, and the visible vector is in cyan. They create the 3 surfaces shown in red, green, and blue, whose normals are  $B_i$ , blue, and  $S_i$ , red.

Next, we have the algorithm to determine the arm's placement in space relative to the joint limits seen in Fig. 3 (B). The first step in the algorithm determines which internal surfaces the arm lies between. A vector is created from the flexion and abduction angles of the arm. The raw values of the motors are intrinsic angles, and the clinically relevant angles are extrinsic. Normally, a Jacobian transform is applied; however, this design uses a single joint center, making the Jacobian a rotation matrix, without the need for linearization as shown in ???. This rotation is applied to convert the motor angles to human joint angles used in the reach cone space. The transformed angles are then used to form the vector  $L$ . Then a dot product is taken with each  $S_i$  until the conditions describing its containment between consecutive planes are met. This condition is shown below and in 3 (B), boxed in red.

$$S_i \cdot L \geq 0 \text{ and } S_{i+1} \cdot L \leq 0 \quad (4)$$

The last step is to calculate whether the arm is within the wedge using the outer surface corresponding to this particular wedge,  $B_i$ . This dot product also produces the linear distance from the outer surface,  $d$ , as all surfaces and vectors share a common point, which is the joint center. If  $d$  is positive, the arm is within the reach cone; if the value is negative, the arm is outside the reach cone.

To produce the proper virtual forces in the component directions of the motors, the distance  $d$  will need to be converted to  $\theta_e$  for each of the flexion and abduction directions. To do this  $L$  is projected onto  $B_i$  and normalized, shown below:

$$L_B = \text{proj} \rightarrow L \rightarrow B_i = \frac{L - (L \cdot B_i)B_i}{\|L - (L \cdot B_i)B_i\|} \quad (5)$$

Next, the angle between the original and projected vector is calculated to get the angle needed to rotate the vector onto the reach cone. The last step is to get the axis about which the vector must be rotated to get the full angle-axis rotation transform. This vector will give the rotation about each orthogonal axis. These equations are shown below:

$$\beta = \cos^{-1}(L \cdot L_B) \quad (6)$$

$$a = L \times L_B \quad (7)$$

## B. Mechanical

The base system from the original submission [11] has been augmented to work with our Franka Panda robotic manipulators. The original motors were swapped out for Maxon 647697 motors. These motors were selected for their high torques and low friction. While humans can perceive the cogging in these motors, the cogging is imperceptible to the manipulator's sensors.

## C. Electronics

Upgrades made to the previous system, [11] include: switching to a Raspberry Pi, O Drive Pro motor controllers for the brushless motors.

## D. Software

The upgrades to our electronic system have allowed us to implement new control schemes. Specifically, we have implemented torque control that allows us to reflect the torque of a human tendon more accurately. The torque control equation is as follows:

$$K_p(\theta_e) = -0.002\theta_e^2 + 0.081\theta_e - 0.093 \quad (8)$$

$$\tau = ({}^m_s \mathcal{R} K_p(\theta_e)) \odot \theta_e - b {}^m_s \mathcal{R} \dot{\theta}_e \quad (9)$$

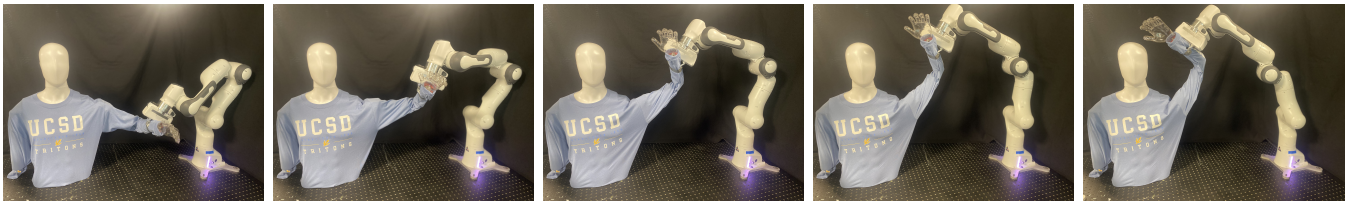


Fig. 4: The series of images above shows snapshots of a trajectory in which the Franka Panda arm can move the SHULDRD through a significant range of motion limited by the Franka arm’s reachable space. In this trajectory, the Franka arm has its default gripper holding the arm. In other trajectories, a load cell and three-finger gripper (Right-hand) were used to validate the ability to sense the resistive torques of the motors.

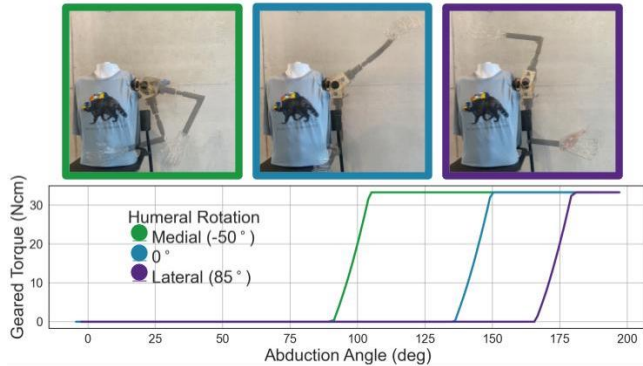


Fig. 5: The graph above shows multiple trials moving the SHULDRD with increasing humeral rotation. The motor torque (Ncm) is graphed against the device’s measured angle (deg). It shows how the change in configuration changes the activation angle of the motors, simulating the transition to new joint limits.

### III. EXPERIMENTS AND SIMULATIONS

#### A. Humeral Joint Coupling Experiment

A key biomechanical aspect of the shoulder complex is the coupled nature of the joint limits in each DOF. To validate the SHULDRD’s ability to replicate this behavior, the device was moved in a repeated arc constrained to pure abduction while changing the humeral angle for each trial and observing the onset of motor torque activation. The internal encoders were used to measure the real-time position of both the humeral and abduction rotations, and the commanded output torque was recorded.

As shown in Fig. 5, the device activates the motors at different abduction angles dependent on the humeral rotation as the device transitions between joint limits. A  $-50^\circ$  internal rotation of the humerus gave the smallest range of motion at  $90^\circ$ . An external rotation of  $80^\circ$  gave the largest range at  $165^\circ$ .

#### B. pHRI: using the SHULDRD as a human subject

The Franka Panda robotic manipulator, the ATI Axia80 M8 transducer force-torque sensor, and two different grippers were used to manipulate the SHULDRD. The manipulator was positioned to grasp the arm and given a waypoint trajectory to move the device. The path was chosen to activate the virtual tendons and return the free range of motion. The time series images for one of the trajectories, with the Franka and native gripper, can be seen in Fig. 4. The force-torque sensor, when integrated, was capable of sensing the resistive torques of the virtual joint limits (haptics vs.

no haptics) in a manipulation task. This comparison of data from passive and active motors is shown in Fig. 1.

### IV. DISCUSSION AND CONCLUSIONS

In this paper, the device replicates the essential parts of human shoulder motion, and the limitations necessary for real-world planning and learning algorithms meant to enhance safety for human-robot physical interaction. The SHULDRD shows the ability to measure its angular position and provide accurate complex joint constraints, tendon forces, and damping, which mimic the biological constraints and parameters.

Some inaccuracies in the modeling include the magnitude of the forces, which were chosen at a much lower maximum torque for user safety and use with smaller, more affordable manipulator platforms. Larger motors and more expensive motor drivers could replace the current electronics to increase sensing capabilities and output torque.

As with all robotics systems, it is important to understand where singularities might exist. In the SHULDRD, the minimum set of actuators was chosen to cover 3 degrees of freedom. While this afforded the device simplicity and exact transforms, there is a singularity at  $90^\circ$  abduction when the humeral rotation and flexion axes are aligned, which inhibits some trajectories.

Future applications of this work include testing path-planning algorithms to help with self-feeding, dressing, search and rescue, and telemedicine to ensure safety without risk to human subjects. This should increase the ability to test learning algorithms that require large amounts of data and trials to run properly, and test algorithms that do safe exploring near the end range of motion for the shoulder.

## REFERENCES

- [1] Y. Wang, Z. Sun, Z. Erickson, and D. Held, "One policy to dress them all: Learning to dress people with diverse poses and garments," *arXiv preprint arXiv:2306.12372*, 2023.
- [2] B. Roy, A. Basmajian, and H. Asada, "Maneuvering a bed sheet for repositioning a bedridden patient," in *2003 IEEE International Conference on Robotics and Automation (Cat. No.03CH37422)*, vol. 2, pp. 2224–2229 vol.2, 2003.
- [3] A. H. Ali, S. M. H. Kazmi, and R. Uddin, "Tele-operated robotic manipulator based contactless heartbeat measurement mechanism," in *2023 International Conference on Robotics and Automation in Industry (ICRAI)*, pp. 1–6, 2023.
- [4] B. A. Frederiksen, M. Schousboe, L. Terslev, N. Iversen, H. Lindgaard, T. R. Savarimuthu, and S. A. Just, "Ultrasound joint examination by an automated system versus by a rheumatologist: from a patient perspective," *Advances in Rheumatology*, vol. 62, p. 30, 2022.
- [5] R. Tejwani, C. Ma, P. Gomez-Paz, P. Bonato, and H. Asada, "Demonstrating language-grounded motion controller,"
- [6] E. Peiros, Z.-Y. Chiu, Y. Zhi, N. Shinde, and M. C. Yip, "Finding biomechanically safe trajectories for robot manipulation of the human body in a search and rescue scenario," in *2023 IEEE/RSJ International Conference on Intelligent Robots and Systems (IROS)*, pp. 167–173, IEEE, 2023.
- [7] Y. He, D. Eguren, T. P. Luu, and J. L. Contreras-Vidal, "Risk and adverse events related to lower-limb exoskeletons," in *2017 International Symposium on Wearable Robotics and Rehabilitation (WeRob)*, pp. 1–2, IEEE, 2017.
- [8] Q. Zhao, R. Roy, C. Spurlock, K. Lister, and L. Wang, "A high-fidelity simulation framework for grasping stability analysis in human casualty manipulation," *arXiv preprint arXiv:2404.03741*, 2024.
- [9] N. B. Reese and W. D. Bandy, *Joint range of motion and muscle length testing-E-book*. Elsevier Health Sciences, 2016.
- [10] J. Wilhelms and A. V. Gelder, "Fast and easy reach-cone joint limits," *Journal of graphics tools*, vol. 6, no. 2, pp. 27–41, 2001.
- [11] E. Peiros, C. Joyce, T. Murugesan, R. Nguyen, I. Fiorini, R. Galibut, and M. C. Yip, "Haptic shoulder for rendering biomechanically accurate joint limits for human-robot physical interactions," 2024.